Comput Geosci (2013) 17:773–788
DOI 10.1007/s10596-013-9355-1

Controllability and observability in two-phase porous media flow

Jorn F. M. Van Doren · Paul M. J. Van den Hof · Okko H. Bosgra · Jan Dirk Jansen

Received: 22 March 2013 / Accepted: 6 May 2013 / Published online: 28 June 2013

Abstract Reservoir simulation models are frequently used to make decisions on well locations, recovery optimization strategies, etc. The success of these applications is, among other aspects, determined by the controllability and observability properties of the reservoir model. In this paper, it is shown how the controllability and observability of two-phase flow reservoir models can be analyzed and quantified with aid of generalized empirical Gramians. The empirical controllability Gramian can be interpreted as a spatial covariance of the states (pressures or saturations) in the reservoir resulting from input perturbations in the wells. The empirical observability Gramian can be interpreted as a spatial covariance of the measured bottom-hole pressures or well bore flow rates resulting from state perturbations. Based on examples in the form of simple homogeneous and heterogeneous reservoir models, we conclude that the position of the wells and of the front between reservoir fluids, and to a lesser extent the position and shape of permeability heterogeneities that impact the front, are the most important factors that determine the local controllability and observability properties of the reservoir.

Keywords Reservoir engineering · Reservoir simulation · Controllability · Observability · Two-phase flow · Porous media · Empirical Gramians · Covariance matrix · Proper orthogonal decomposition · POD

J. F. M. Van Doren · O. H. Bosgra
Delft Center for Systems and Control,
Delft University of Technology,
Postbus 5, 2600 AA Delft, The Netherlands

P. M. J. Van den Hof
Department of Electrical Engineering,
Eindhoven University of Technology,
Den Dolech 2, 5612 AZ Eindhoven, The Netherlands

J. D. Jansen (✉)
Department of Geoscience and Engineering,
Delft University of Technology,
Postbus 5048, 2600 GA Delft, The Netherlands
e-mail: j.d.jansen@tudelft.nl

Nomenclature

$\mathbf{A}$	System matrix
$\mathbf{B}$	Input matrix
c	Compressibility, or constant
$\mathbf{C}$	Output matrix
$\mathcal{C}$	Controllability matrix
d	Depth
$\mathbf{D}$	Direct throughput matrix
$\mathbf{e}$	Unit vector
$\mathscr{E}$	Set of unit vectors
f	Fractional flow
$\mathbf{f}$	Vector-valued function
$\mathbf{F}$	Fractional flow matrix
g	Acceleration of gravity
$\mathbf{h}$	Vector-valued function
$\mathbf{I}$	Identity matrix
$\mathbf{J}$	Well index matrix
k	Permeability, or discrete time
K	Total number of time steps
$\mathbf{K}$	Permeability tensor
m	Number of inputs (size of $\mathbf{u}$)
M	Subset of $\mathbb{R}^m$
$\mathscr{M}$	Set of positive constants
n	Number of states (size of $\mathbf{x}$)
N	Subset of $\mathbb{R}^n$

$\mathcal{O}$ Observability matrix
p Pressure, or number of outputs (size of $\mathbf{y}$)
$\mathbf{p}$ Pressure vector
P Subset of $\mathbb{R}^p$
$\mathcal{P}$ Controllability Gramian
q Flow rate
q''' Flow rate per unit volume
$\mathbf{q}$ Flow rate vector
$\mathcal{Q}$ Observability Gramian
r Number of elements in $\mathcal{T}$
s Number of snapshots, or number of elements in $\mathcal{M}$
S Saturation
$\mathbf{s}$ Saturation vector
t Time
T Temperature
$\mathbf{T}$ Transmissibility matrix, or orthonormal matrix, or transformation matrix
$\mathcal{T}$ Set of orthonormal matrices
$\mathbf{u}$ Input vector, or left singular vector
$\mathbf{U}$ Matrix of input vectors, or matrix of left singular vectors
$\mathbf{V}$ Accumulation matrix, or matrix of right singular vectors
$\mathbf{x}$ State vector
$\mathbf{y}$ Output vector
z Number of elements in "weighted singular vector"
$\mathbf{\Gamma}$ Diagonal scaling matrix
λ Eigenvalue
μ Viscosity
ρ Density
σ Singular value
$\mathbf{\Sigma}$ Diagonal matrix of singular values
ϕ Porosity
$\mathbf{\Phi}$ Auxiliary matrix
$\mathbf{\Psi}$ Auxiliary matrix

Subscripts

c Capillary, or continuous-time
e Empirical
o Oil
op Oil pressure
os Oil saturation
p Pressure
r Rock
ro Relative, oil
rw Relative, water
s Saturation
t Total
u Input
y Output
w Water
wp Water pressure
ws Water saturation

Superscripts

T Transpose

1 Introduction

In an earlier paper [1], we analyzed several system-theoretical aspects of single-phase flow through porous media. In particular, we addressed single-phase, slightly compressible flow. In that case, the dynamic system behavior can be described with linear differential equations in terms of a single state variable (dynamic variable), i.e., pressure, which is a function of space and time. As a typical system parameter (static variable), we considered permeability, which is a function of space only. As system inputs (controls), we considered prescribed flow rates or bottom-hole pressures in the wells, while as system outputs (measurements), we took the bottom-hole pressures in those wells where the rates were prescribed and vice versa. For such a setup, *controllability* can be defined, loosely speaking, as the extent to which we can influence the state variables at any particular point in the reservoir by manipulating the inputs. *Observability* can be defined as the extent to which we reconstruct the state variables at any particular point in the reservoir from the outputs. *Identifiability* is the extent to which we can reconstruct parameter values at any particular point from input–output data. In the present paper, we will extend our earlier analysis to controllability and observability of slightly compressible two-phase (oil–water) flow. Unlike the case of single-phase flow which leads to linear equations, the two-phase case is nonlinear, which complicates the analysis. Moreover, whereas the equations for single-phase flow are diffusive, we are now considering combined diffusive–convective behavior of coupled pressures and saturations which causes further complications.

Controllability is of relevance for the optimization of flooding processes, see e.g., [1–7], while observability and identifiability are of relevance to state and parameter estimation in computer-assisted history matching; see e.g., [1, 8–13]. Moreover, the concepts of controllability and observability can be used to quantify those parts of a reservoir model that are most important to the input–output behavior, which offers scope to reduce the computational complexity through control-relevant upscaling [14, 15]. The concepts are also closely related to reduced-order modeling with the aid of proper orthogonal decomposition (POD) although the link is not always explicitly mentioned in the papers

concerned; see e.g., [16–18]. Traditionally, controllability, observability, and identifiability are considered to be qualitative measures, i.e., they provide yes/no answers to the question if a system is controllable/observable/identifiable over the full spatial domain. However, this presupposes the availability of controls that can provide arbitrarily strong input signals, and sensors that can observe arbitrarily weak output signals. This is clearly unrealistic, and therefore it is more meaningful to use a quantitative measure. Using such a quantitative measure, we showed in our earlier paper that the extent to which the reservoir pressures are controllable and observable is very limited, and restricted to pressures in areas close to the wells. Although we did not analyze identifiability in detail, we showed a close relationship between the identifiability of permeabilities, and the observability of pressures, such that the same conclusion hold, i.e., permeabilities can only be identified to a very limited extent. Further aspects of the identifiability of permeabilities in single-phase flow, and its relation to observability and controllability, are given in [11, 12]. Moreover, the identifiability of reservoir parameters from measured data is closely related to the ability to compute "sensitivities" of measured data to reservoir parameters. This is an important topic for computer-assisted history matching or well testing, about which, therefore, exist many publications. However, most of the literature on sensitivities is focused on computational aspects; see e.g., [19–21]. A much smaller number of authors has addressed identifiability, or related concepts such as resolution or information content. For a recent discussion, see [13]; for specific papers, see e.g., [8, 9, 11, 12]. Although the identifiability of parameters, or related concepts, has been treated before, to our knowledge, very few papers have been published on controllability and observability of state variables in reservoir flow. We are aware of two publications that address the controllability of pressures in single-phase flow [1, 4], where the latter is restricted to homogeneous reservoirs, and of two publications that address the controllability of saturations (oil–water fronts) in two-phase flow [3, 6]. However, the latter only treat the special case of incompressible flow of two near-identical fluids using the theory of potential flow. Here, we present a general technique to analyze and quantify the (local) controllability and observability of pressures and saturations in multiphase flow.

2 Controllability and observability for nonlinear models

2.1 Introduction

In the Appendix, a brief derivation of the equations is presented for two-phase flow through porous media in state-space form. The resulting equations are the (differential) *state equations*

$$\mathbf{x}_{k+1} = \mathbf{A}(\mathbf{x}_k)\,\mathbf{x}_k + \mathbf{B}(\mathbf{x}_k)\,\mathbf{u}_k, \quad k = 0, 1, ..., K-1, \tag{1}$$

and the (algebraic) *output equations*

$$\mathbf{y}_k = \mathbf{C}(\mathbf{x}_k)\,\mathbf{x}_k + \mathbf{D}(\mathbf{x}_k)\,\mathbf{u}_k, \tag{2}$$

where $\mathbf{x}_k = \begin{bmatrix}\mathbf{p}_k^T & \mathbf{s}_k^T\end{bmatrix}^T \in N \subset \mathbb{R}^n$ is a vector of state variables (i.e., of grid block pressures $\mathbf{p}_k$ and grid block saturations $\mathbf{s}_k$), $\mathbf{u}_k \in M \subset \mathbb{R}^m$ is a vector of inputs (pressures, total flow rates, or valve settings in the wells), $\mathbf{y}_k \in P \subset \mathbb{R}^p$ is a vector of measurements (pressures or phase rates in the wells), k is the discrete-time index, and K is the total number of time steps. The sets M, N, and P are subsets of $\mathbb{R}^m$, $\mathbb{R}^n$, and $\mathbb{R}^p$, respectively because their elements are constrained to stay within physical limits; e.g., pressures are always positive and saturations have values between 0 and 1. To simplify the notation, we will from now on define all variables as members of $\mathbb{R}^x$ with x an appropriate dimension, where the necessary subsets are to be tacitly understood. The state-dependent matrices $\mathbf{A}(\mathbf{x}_k) \in \mathbb{R}^{n\times n}$, $\mathbf{B}(\mathbf{x}_k) \in \mathbb{R}^{n\times m}$, $\mathbf{C}(\mathbf{x}_k) \in \mathbb{R}^{p\times n}$, and $\mathbf{D}(\mathbf{x}_k) \in \mathbb{R}^{p\times m}$ are given by expressions (66) to (69) with details in equations (50) to (53).

2.2 Nonlinearity of two-phase flow equations

Equations 1 and 2 are nonlinear because of various dependencies of the coefficients on the state variables $\mathbf{x}_k$ such as, e.g., the dependency of the relative permeabilities on saturations, and of the fluid compressibilities and densities, and rock porosity on pressures. The equations are *control-affine*, because the inputs $\mathbf{u}_k$ enter the equations linearly. (An affine function is a linear function plus a translation. Control-affine functions are an important topic of study in nonlinear control theory.). We note that although we present the theory in explicit discrete-time notation (for notational convenience), the results that follow do not depend on implicit or explicit time discretization or on the particular value of the discretization time step, and also apply to the continuous-time case. The nature of two-phase flow equations is much more complex than that of the single-phase equations. The latter describe a pressure field that is diffusive, i.e., the corresponding equations are parabolic and become elliptic in the limit of zero compressibility. However, the two-phase equations describe both pressures and saturations. The pressures $\mathbf{p}_k$ behave similarly as in the single-phase case although somewhat modified by two-phase effects, but the saturations $\mathbf{s}_k$ behave completely different and can be characterized as diffusive–convective, i.e., their corresponding equations are mixed parabolic–hyperbolic and become completely hyperbolic in the case of zero capillary pressure.

From a control perspective, this implies a markedly different dynamic behavior. In the single-phase case, the dynamic response of the autonomous equations (i.e., without inputs $\mathbf{u}_k$) to a small disturbance (in the form of an initial condition $\mathbf{x}_0$) from an equilibrium situation (constant pressures in two horizontal dimensions, or hydrostatic pressures in three dimensions) results in a return to the equilibrium situation. However, in the two-phase case, the saturations are driven by convection (which is governed by the spatial distribution of the pressures), and a small disturbance (in the pressures and/or the saturations) from an equilibrium situation will result in a permanent small change in the saturations. Correspondingly, the eigenvalues of a continuous-time linear (or linearized) single-phase system have real negative values (the fact that they are real implies that the response is nonoscillatory because inertia does not play a role in the governing equations), whereas only half of the eigenvalues of a linearized two-phase system are real and negative (for the pressures states) while the other half are equal to 0 (for the saturation states). The two-phase response is therefore still bounded and nonoscillatory. In other words, the single-phase system equations are asymptotically stable, whereas the linearized two-phase equations are only Lyapunov stable.

Another difference between single-phase and two-phase flow is in the steady-state behavior of the system. In the single-phase case, steady-state flow may occur after dampening out of the pressure transients. However, the effect of the convective behavior of the saturations is that there does not exist any nontrivial two-phase steady-state solution for inputs that result in flow (i.e., that produce a nonhydrostatic pressure gradient). This is because flow produces (very slow) saturation changes as long as there are two mobile phases present. (The trivial solution occurs when all mobile oil has been flushed out of the reservoir which effectively makes the reservoir single phase.) The typical timescale for pressure changes (e.g., defined as the half time for dampening out of an impulsive pressure disturbance in a well) is very small (typically in the order of hours to days) compared to the time for saturation changes to propagate through the entire reservoir (typically in the order of years to decades). Therefore, it is usually justified to consider the saturation field to be very slowly time-varying. The pressure response is then governed by linear equations with (very slowly) time-varying coefficients, and, after dampening out of pressure transients resulting from initial conditions, may be considered to be in near-steady state.

2.3 Controllability and observability

For formal definitions of the controllability and observability of nonlinear models, we refer to [22]. Here, we will present a practical approach to analyze and quantify the controllability and observability in a reservoir simulation setting. Reservoir models are large-scale and hence have a large number of state variables. Consequently, not all approaches to analyze the controllability and observability of nonlinear models are currently computationally feasible for this application area. Examples of methods that are currently not feasible are the nonlinear local controllability and observability analysis with a differential geometric approach [23] and the application of the nonlinear controllability and observability function [24]. However, there are other approaches that can be used. The first one is to linearize the model equations around a steady-state operating point and analyze the linearized model with controllability and observability tools for linear time-invariant (LTI) models, or to linearize them along a nominal state trajectory (i.e., a sequence of state vectors in time) and analyze the model with controllability and observability tools for linear time-varying (LTV) systems. The second approach is to use empirical Gramians [25, 26] to approximate the controllability and observability Gramians of nonlinear models. Empirical Gramians can be computed for nonlinear large-scale models such as reservoir models. All these methods are "local" in the sense that they only address the controllability observability of state variables in the neighborhood of the linearization point or trajectory, i.e., for small changes in the inputs and initial conditions compared to the values used for the linearization. Here, we will use the empirical Gramian approach.

2.4 Controllability Gramian interpreted as covariance matrix

Recall that a discrete-time LTI system,

$$\mathbf{x}_{k+1} = \mathbf{A}\mathbf{x}_k + \mathbf{B}\mathbf{u}_k, \quad k = 0, 1, \ldots, K-1, \tag{3}$$

is controllable if its controllability matrix,

$$\mathcal{C} \in \mathbb{R}^{n\times n} \triangleq \begin{bmatrix} \mathbf{B} & \mathbf{AB} & \mathbf{A}^2\mathbf{B} & \cdots & \mathbf{A}^{k-1}\mathbf{B} \end{bmatrix} \tag{4}$$

has full rank (see e.g., [27]). This is equivalent to requiring that the controllability Gramian,

$$\mathcal{P} \in \mathbb{R}^{n\times n} \triangleq \mathcal{C}\mathcal{C}^T = \sum_{k=0}^{K-1} \mathbf{A}^k\mathbf{B}\mathbf{B}^T \left(\mathbf{A}^T\right)^k, \tag{5}$$

has full rank. (Note that we make no distinction between "reachability" to reach a state starting from an initial condition, or "controllability" to drive back a state to a zero condition, because these concepts lead to identical requirements for a discrete-time formulation). In a reservoir simulation setting, Eq. 3 represents a single-phase reservoir model or a linearized version of a multiphase reservoir model; see Eqs. 70 and 71 in the Appendix, from which we dropped the

overbars to simplify the notation. An interpretation of Eq. 5 can be obtained by rewriting Eq. 3 as a recursive sequence:

$$\begin{aligned}
\mathbf{x}_1 &= \mathbf{A}\mathbf{x}_0 + \mathbf{B}\mathbf{u}_0,\\
\mathbf{x}_2 &= \mathbf{A}^2\mathbf{x}_0 + \mathbf{A}\mathbf{B}\mathbf{u}_0 + \mathbf{B}\mathbf{u}_1,\\
\mathbf{x}_3 &= \mathbf{A}^3\mathbf{x}_0 + \mathbf{A}^2\mathbf{B}\mathbf{u}_0 + \mathbf{A}\mathbf{B}\mathbf{u}_1 + \mathbf{B}\mathbf{u}_2,\\
&\vdots\\
\mathbf{x}_K &= \mathbf{A}^K\mathbf{x}_0 + \mathbf{A}^{K-1}\mathbf{B}\mathbf{u}_0 + \ldots + \mathbf{A}\mathbf{B}\mathbf{u}_{K-2} + \mathbf{B}\mathbf{u}_{K-1}.
\end{aligned} \tag{6}$$

Starting from an initial condition $\mathbf{x}_0 = \mathbf{0}$, and a unit impulse input at time 0, i.e., $\mathbf{u}_0 = \mathbf{1}$; $\mathbf{u}_1 = \mathbf{u}_2 = \ldots = \mathbf{u}_{k-1} = \mathbf{0}$, where $\mathbf{1}$ is a vector of unit length, it follows that

$$\mathbf{x}_k^{'} = \mathbf{A}^{k-1}\mathbf{B}, \tag{7}$$

where the accent indicates that the response results from a unit impulse input. Equation 5 can therefore be written as

$$\mathcal{P} = \sum_{i=1}^{K} \mathbf{x}_i^{'} \left(\mathbf{x}_i^{'}\right)^T = \left[\begin{array}{cccc} \mathbf{x}_1^{'} & \mathbf{x}_2^{'} & \cdots & \mathbf{x}_K^{'} \end{array}\right] \left[\begin{array}{c} \mathbf{x}_1^{'T} \\ \mathbf{x}_2^{'T} \\ \vdots \\ \mathbf{x}_K^{'T} \end{array}\right]. \tag{8}$$

Next, consider the definition of the (sample) covariance between elements of the state vector $\mathbf{x}$:

$$Cov\,(\mathbf{x},\mathbf{x}) \in \mathbb{R}^{n\times n} \triangleq \frac{1}{s-1}\left[\begin{array}{cccc} \widetilde{\mathbf{x}}_1 & \widetilde{\mathbf{x}}_2 & \cdots & \widetilde{\mathbf{x}}_s \end{array}\right] \left[\begin{array}{c} \widetilde{\mathbf{x}}_1^T \\ \widetilde{\mathbf{x}}_2^T \\ \vdots \\ \widetilde{\mathbf{x}}_s^T \end{array}\right], \tag{9}$$

where s is the sample size, i.e., the number of state vector "snapshots" in time used to estimate the covariance, and $\widetilde{\mathbf{x}}$ indicates a (sample) mean-centered snapshot:

$$\widetilde{\mathbf{x}}_i \triangleq \mathbf{x}_i - \frac{1}{s}\sum_{j=1}^{s} \mathbf{x}_j. \tag{10}$$

Comparison of Eqs. 8 and 9 illustrates that the controllability Gramian $\mathcal{P}$ can be interpreted as a generalized spatial covariance matrix of the state response to a unit impulse input. Note that for the Gramian to be full rank, it is required that the number of time steps K is at least as large as the number of states n.

2.5 Empirical controllability Gramian

For a nonlinear state equation, an empirical controllability Gramian can be computed from an ensemble of the state "snapshots" taken from state trajectories corresponding to a set of input signals. The Gramian for a linear system, if full rank, guarantees that any possible combinations of states can be reached from a zero initial condition (although possibly with input signals of unrealistically large magnitudes). An empirical Gramian is less powerful, and, if full rank, only guarantees "local" controllability, i.e., that those combinations of states can be reached that are "close" to the state trajectories used to derive the Gramians. The original derivation of empirical Gramians by Lall et al. [25] is expressed in continuous time. Here, we will follow largely their approach and notation but express the results in discrete time. To compute an empirical controllability Gramian, consider the following auxiliary variables:

1. A set $\mathscr{E}^m = \{\mathbf{e}_1, \mathbf{e}_2, \ldots, \mathbf{e}_m\}$ of standard unit vectors $\mathbf{e}_i \in \mathbb{R}^m$, $i = 1, 2, \ldots, m$,
2. A set $\mathscr{T}^m = \{\mathbf{T}_1, \mathbf{T}_2, \ldots, \mathbf{T}_r\}$ of orthonormal matrices, $\mathbf{T}_l \in \mathbb{R}^m \times m$, $l = 1, 2, \ldots, r$,
3. A set $\mathscr{M}$ of positive constants $c_j \in \mathbb{R}$, $j = 1, 2, \ldots, s$.

With sets $\mathscr{E}^m$, $\mathscr{T}^m$, and $\mathscr{M}$, where m is the number of inputs to the system (i.e., the dimension of $\mathbf{u}$) one can generate a total of $m \times r \times s$ "perturbed" time sequences $\mathbf{U}^{ilj} \in \mathbb{R}^{m\times K}$ of input vectors defined as

$$\mathbf{U}^{ilj} \triangleq \left[\begin{array}{cccc} \mathbf{u}_0^{ilj} & \mathbf{u}_1^{ilj} & \cdots & \mathbf{u}_{K-1}^{ilj} \end{array}\right], \tag{11}$$

where

$$\mathbf{u}_k^{ilj} \triangleq c_j \mathbf{T}_l \mathbf{e}_i \delta_k + \breve{\mathbf{u}}, \quad k = 0, 1, \ldots, K-1, \tag{12}$$

δ_k is the Kronecker delta (defined as $\delta_k = 1$ if $k = 0$, $\delta_k = 0$ if $k \neq 0$), and $\breve{\mathbf{u}}$ is a nominal steady-state input around which the perturbations are taken. The role of the unit vectors is to select each of the components of $\mathbf{u}$ one by one. The matrices $\mathbf{T}_j$ can be used to select different combinations of components, and the constants c_u to select different magnitudes of the perturbations, which may all be of importance because of the nonlinear nature of the system equations. Next, the input sequences $\mathbf{U}^{ilj}$ are used to generate state trajectories, and the empirical controllability Gramian is defined as

$$\mathcal{P}_e \triangleq \sum_{i=1}^{m}\sum_{l=1}^{r}\sum_{j=1}^{s} \frac{1}{rsc_j^2} \sum_{k=1}^{K} \mathbf{\Phi}_k^{ilj}, \tag{13}$$

with the rank-one matrices $\mathbf{\Phi}_k^{ilj} \in \mathbb{R}^{n\times n}$ given by

$$\mathbf{\Phi}_k^{ilj} \triangleq \tilde{\mathbf{x}}_k^{ilj} \left(\tilde{\mathbf{x}}_k^{ilj}\right)^T, \tag{14}$$

where $\tilde{\mathbf{x}}_k^{ilj}$ are mean-centered snapshots as defined in Eq. 10 with $s = K$. If the system is stable, linear, control-affine, and excited with an impulse input, then the empirical controllability Gramian is identical to the controllability Gramian [25, 26]. Hahn et al. [26] extended definition (12) to include other forms of inputs, such as (series of) step inputs, resulting in more general covariance matrices of which empirical Gramians form a subset. (Alternatively, these covariance matrices could be referred to as generalized empirical Gramians). As discussed by Hahn et al. [26], the definition of empirical controllability Gramians is restricted

to control-affine Lyapunov-stable systems starting from a steady-state situation. The first two conditions are met without problems for our two-phase reservoir flow equations. The third one is met approximately because, as discussed in Section 2.2, the saturation changes are typically so slow that the saturation field may be considered to be near-constant and the pressure field to be near-steady-state. In that case, we can compute empirical Gramians (or covariance matrices) by taking "snapshots" of states resulting from perturbed inputs along a (near-steady-state) trajectory in input-state space. This is identical to the typical approach to compute covariance matrices for use in POD.

2.6 Empirical observability Gramian

The observability Gramian for an LTI system (3) observed according to an LTI output equation

$$\mathbf{y}_k = \mathbf{C}\mathbf{x}_k + \mathbf{D}\mathbf{u}_k, \tag{15}$$

is observable if its observability matrix,

$$\mathcal{O} = \begin{bmatrix} \mathbf{C} \\ \mathbf{CA} \\ \mathbf{CA}^2 \\ \vdots \\ \mathbf{CA}^{K-1} \end{bmatrix}, \tag{16}$$

is full rank (see e.g., [27]). This is equivalent to requiring that the observability Gramian,

$$\mathcal{Q} \in \mathbb{R}^{n\times n} \triangleq \mathcal{O}^T\mathcal{O} = \sum_{i=0}^{K-1} \left(\mathbf{A}^T\right)^i \mathbf{C}^T\mathbf{C}\mathbf{A}^i, \tag{17}$$

has full rank. For nonlinear systems, an empirical observability Gramian can be defined which can be interpreted as the covariance of the output resulting from a large number of initial state vectors [25]. With the aid of sets $\mathscr{E}^n$, $\mathscr{T}^n$, and $\mathscr{M}$ as defined above, where n is the number of state variables (i.e., the dimension of $\mathbf{x}$), one can generate a total of $n \times r \times s$ initial state vectors $\mathbf{x}_0^{ilj} \in \mathbb{R}^n$ defined as

$$\mathbf{x}_0^{ilj} \triangleq c_j \mathbf{T}_l \mathbf{e}_i + \breve{\mathbf{x}}_0, \tag{18}$$

where $\breve{\mathbf{x}}_0$ is a nominal initial condition around which the perturbations are taken. Next, the initial conditions are used, with zero inputs, to generate states and outputs and the empirical observability Gramian is defined as

$$\mathcal{Q}_\mathrm{e} \triangleq \sum_{l=1}^{r}\sum_{j=1}^{s} \frac{1}{rsc_j^2} \sum_{k=0}^{K-1} \mathbf{T}_l \boldsymbol{\Psi}_k^{lj} \mathbf{T}_l^T, \tag{19}$$

in which the elements $\Psi_{iu,k}^{lj}$ of matrix $\boldsymbol{\Psi}_k^{lj} \in \mathbb{R}^{n\times n}$ are given by

$$\Psi_{iu,k}^{lj} = \left(\tilde{\mathbf{y}}_k^{ilj}\right)^T \left(\tilde{\mathbf{y}}_k^{ulj}\right), \tag{20}$$

where $\tilde{\mathbf{y}}_k^{ulj}$ are mean-centered outputs of the system. If the system is stable and linear, then the empirical observability Gramian is identical to the observability Gramian [25]. The empirical observability Gramian is calculated based on the outputs of the model for a large number ($n \times r \times s$) initial conditions. For applications with a large number of states, this approach is computationally very demanding, because of the need to perform a large number of simulations and to store all corresponding output vectors. References [28] and [29] therefore present an alternative approach to approximate the observability Gramian by taking snapshots of a dual linearized system (a.k.a. an adjoint system), which is computationally much more efficient if the number of outputs p is much smaller than the number of states n (as is usually the case). In the present paper, we followed the latter approach.

2.7 Balancing and Hankel singular values

A state that is sensitive to inputs, i.e., that is strongly controllable, is not necessarily also strongly observable, or vice versa, an effect that is also reflected in the difference between the corresponding (empirical) Gramians. However, it is possible to find a linear "balancing" coordinate transformation $\tilde{\mathbf{T}}$ of the (empirical) Gramians $\mathcal{P}$ and $\mathcal{Q}$ such that the transformed Gramians $\tilde{\mathcal{P}}$ and $\tilde{\mathcal{Q}}$ are equal diagonal matrices that satisfy

$$\tilde{\mathcal{P}} = \tilde{\mathbf{T}}\mathcal{P}\tilde{\mathbf{T}}^T, \tag{21}$$

$$\tilde{\mathcal{Q}} = \tilde{\mathbf{T}}^{-T}\mathcal{Q}\tilde{\mathbf{T}}^{-1}, \tag{22}$$

and

$$\tilde{\mathcal{P}}\tilde{\mathcal{Q}} = \tilde{\mathbf{T}}\mathcal{P}\mathcal{Q}\tilde{\mathbf{T}}^{-1}. \tag{23}$$

The transformation matrix $\tilde{\mathbf{T}}$ can then also be used to define transformed (balanced) states $\tilde{\mathbf{x}} = \tilde{\mathbf{T}}\mathbf{x}$ such that states that are strongly controllable are also strongly observable and vice versa, which implies that they are important to the input–output behavior. Although (empirical) Gramians themselves are coordinate-dependent, the eigenvalues of their product are not. The latter are called the Hankel singular values, and are defined as

$$\sigma_i \triangleq \sqrt{\lambda_i\left(\mathcal{P}\mathcal{Q}\right)} = \sqrt{\lambda_i\left(\tilde{\mathcal{P}}\tilde{\mathcal{Q}}\right)}, \quad i = 1, 2, \ldots, n. \tag{24}$$

If the Hankel singular values decrease rapidly, this is an indication that the input–output behavior is determined by only the first few balanced states. For details about balancing, see e.g., Moore [30] (the original paper), Antoulas [31] (a textbook), or [1] (an application to single-phase flow; our earlier paper).

3 Quantifying controllability and observability

3.1 Singular value decompositions

To quantify observability and controllability, singular value decompositions (SVDs) can be used to compute subspaces that are most controllable or observable. In reference [1], we applied this method to single-phase porous media flow, and we will use the same approach here for two-phase flow using empirical Gramians. The controllable states (i.e., the subspace $X^{con} = \mathrm{Im}(\mathcal{C})$) can be approximated by using an approximate version of $\mathcal{C}$ defined as

$$\mathcal{C} = \mathbf{U}\mathbf{\Sigma}\mathbf{V}^T = \begin{bmatrix} \mathbf{U}_1 & \mathbf{U}_2 \end{bmatrix} \begin{bmatrix} \mathbf{\Sigma}_1 & \mathbf{0} \\ \mathbf{0} & \mathbf{\Sigma}_2 \end{bmatrix} \begin{bmatrix} \mathbf{V}_1^T \\ \mathbf{V}_2^T \end{bmatrix} \approx \mathbf{U}_1\mathbf{\Sigma}_1\mathbf{V}_1^T, \tag{25}$$

where the separation between $\mathbf{\Sigma}_1$ and $\mathbf{\Sigma}_2$ is chosen in such a way that the singular values in $\mathbf{\Sigma}_2$ are considerably smaller than those in $\mathbf{\Sigma}_1$. The first few left singular vectors, i.e., the first few columns of $\mathbf{U}_1$, are now just the most controllable linear combinations of states. Alternatively, an SVD can be applied to the controllability Gramian,

$$\mathcal{P} = \mathcal{C}\mathcal{C}^T = \mathbf{U}\mathbf{\Sigma}^2\mathbf{U}^T, \tag{26}$$

or to the empirical controllability Gramian $\mathcal{P}_\mathrm{e}$, resulting in the same matrices $\mathbf{U}$ and $\mathbf{\Sigma}$ as in Eq. 25.

The observable states (i.e., the orthogonal complement to the unobservable subspace $X^{unobs} = \mathrm{Ker}(\mathcal{O})$) can be approximated by applying an SVD to the transpose of the observability matrix $\mathcal{O}^T$,

$$\mathcal{O}^T = \mathbf{U}\Sigma\mathbf{V}^T \approx \mathbf{U}_1\mathbf{\Sigma}_1\mathbf{V}_1^T, \tag{27}$$

or, alternatively, to the transpose of the (empirical) observability Gramian $\mathcal{Q}$,

$$\mathcal{Q} = \mathcal{O}^T\mathcal{O} = \mathbf{U}\mathbf{\Sigma}^2\mathbf{U}^T. \tag{28}$$

In this case, the first few columns of $\mathbf{U}_1$ are just the most observable linear combinations of states. Note that the values of $\mathbf{U}$, $\mathbf{\Sigma}$ and $\mathbf{V}$ in Eqs. 25 and 27 are usually not identical, and the same holds for those values in Eqs. 26 and 28.

In a similar fashion, it is possible to determine the SVD of the product of the balanced Gramians $\tilde{\mathcal{P}}\tilde{\mathcal{Q}}$. The first few left singular vectors are in this case the linear combinations of states that contribute most to the input–output behavior of the system.

3.2 Scaling

Consider the case in which the controllable subspace is approximated by removing columns $\mathbf{U}_2$ in $\mathbf{U}$ which correspond to (very) small singular values. In case the values of the input variables vary several orders of magnitude, the values of the input matrix $\mathbf{B}$ related to those inputs influence the numerical values that occur in $\mathbf{\Sigma}_1$ and $\mathbf{\Sigma}_2$, and as such can influence the separation between $\mathbf{\Sigma}_1$ and $\mathbf{\Sigma}_2$. In order to make the selection mechanism scaling-independent, matrix $\mathbf{B}$ can be scaled to

$$\overline{\mathbf{B}} = \mathbf{B}\mathbf{\Gamma}_\mathrm{u}, \tag{29}$$

where $\mathbf{\Gamma}_\mathrm{u} = \mathrm{diag}(\,|u_1| \quad |u_2| \quad \cdots \quad |u_m|\,)^{-1}$, with u_i, $i = 1, 2, \ldots, m$, representing typical (nominal) input values. Alternatively, the values can be scaled with respect to the well indices, as will be discussed below. Subsequently, the controllability matrix and Gramians are calculated. This is illustrated in the next section in which examples are presented where the inputs contain pressures that have values in the range of 10^7 Pa and rates that have values in the range of 1 m^3/s. The same reasoning also applies to the output variables. In order to make the selection mechanism scaling-independent, matrix $\mathbf{C}$ can be scaled to

$$\overline{\mathbf{C}} = \mathbf{\Gamma}_\mathrm{y}\mathbf{C}, \tag{30}$$

where, in this paper, $\mathbf{\Gamma}_\mathrm{y} = \mathrm{diag}(\,|y_1| \quad |y_2| \quad \cdots \quad |y_p|\,)^{-1}$, with y_i, $i = 1, 2, \ldots, p$, representing typical output values.

3.3 Time-varying controllability

The controllability and observability properties of a nonlinear model can change with time, i.e., states can become more or less controllable or observable with time. In this paper, we have therefore chosen to analyze these properties per time interval. To this end, the total simulation time of K time steps is split into intervals $k_{i,f} = [k_i, k_{i+1}, \ldots, k_f]$, where k_i and k_f are the first and last time step of the interval. Subsequently, the controllability of each interval is analyzed. This approach is comparable to the "sliding interval balancing" procedure described in, e.g., reference [32].

3.4 Graphical representation

Each column of $\mathbf{U}$ in Eqs. 25, 26, 27, or 28 contains a singular vector of dimension n, where n is the total number of states. In the case of spatially discretized reservoir models, the states represent grid block pressures and/or grid block saturations. Since each state is connected to a grid block, each column of $\mathbf{U}$ can be interpreted as a set of two spatial patterns (basis functions), representing a pressure field and a saturation field, respectively. The spatial patterns contained in $\mathbf{U}_1$, which correspond to large singular values, are combinations of states that are most controllable or observable. To graphically represent these dominant spatial patterns in a compact way, we have chosen to depict them as a single "weighted singular vector" $\mathbf{u}^z$, consisting of the sum of

the first z singular vectors weighted by their corresponding singular values:

$$\mathbf{u}^z = \sum_{i=1}^{z} \frac{\sigma_i}{\sigma_1} \mathbf{u}_i \tag{31}$$

where σ_i is the ith singular value on the diagonal of $\mathbf{\Sigma}$, and $\mathbf{u}_i$ is the ith column vector of $\mathbf{U}$ (not to be confused with the input vector $\mathbf{u}$). The value of z is chosen such as to maintain 99 % of the total "energy" in the system, i.e., of the sum of all singular values. The weighted singular vectors visualize which parts of the reservoir model contain the dominant, i.e., the most controllable or observable, states. In a geometric interpretation, the columns of the unitary matrix $\mathbf{U}$ represent a direction in the controllable or observable subspace, where the length of the vectors is given by the corresponding singular values. The vectors weighted by their singular value as in Eq. 31 can then be considered as a vector sum, characterizing the dominant directions in the controllable or observable subspace.

4 Controllability and observability of saturations and pressures in two-phase porous media flow

4.1 Introduction

In reference [1], we analyzed the controllability and observability of pressures in single-phase flow. It was concluded that pressures near wells in which the flow rate or bottom-hole pressure can be controlled are most controllable, whereas pressures near wells in which the flow rate or bottom-hole pressure can be measured are most observable. Furthermore, the controllability and observability properties are primarily determined by the well configuration (i.e., the number and location of wells) and to a lesser extent by the heterogeneity of the reservoir. In reference [33], which formed the basis for the present paper, the controllability and observability of saturations in a one-dimensional horizontal reservoir were analyzed. The reservoir was modeled with a linear and nonlinear convection–diffusion equation (CDE) discretized in space and time. Regarding the nonlinear CDE, it was concluded that:

- The saturation states of the nonlinear CDE are most controllable near the oil-water front.
- The saturation states located at the observation point are most observable.
- The saturation states that are most relevant (i.e. least irrelevant) for the input–output behavior are situated around the oil–water front.
- The Hankel singular values decrease rapidly, indicating that reservoir models behave as models of much lower order than the order that follows from the number of grid blocks.

These results are in line with the results of the single-phase controllability and observability analysis in [1]. Additional details on the controllability and observability analysis of the linear and nonlinear CDE can be found in Chapter 3 of [33]. In the remainder of this section, we turn our attention to two-dimensional two-phase reservoir models, where the states are the pressures and saturations in each grid block. Our aim is to identify the dominant grid block pressures and saturations, i.e., those that are most controllable and observable, during the simulation period of the reservoir model.

4.2 Example 1: homogeneous permeability

The first example represents a two-dimensional horizontal homogeneous reservoir in which the oil will be replaced by water in a water-flooding process. The model has $21 \times 21 \times 1$ grid blocks of $10\ \text{m} \times 10\ \text{m} \times 10\ \text{m}$. For the first example, the absolute permeability is $10^{-11}\ \text{m}^2$ in every grid block. The porosity $\phi = 0.30$ and is constant in every grid block. The oil compressibility $c_\text{o} = 10^{-10}\text{Pa}^{-1}$, the water compressibility $c_\text{w} = 10^{-10}\text{Pa}^{-1}$, the oil viscosity $c_\text{o} = 10^{-3}$ Pa s, and the water viscosity $\mu_\text{w} = 10^{-3}$ Pa s. For the relative permeability, the Corey model is used, with Corey exponents $n_\text{o} = n_\text{w} = 2$, $k_{\text{ro},0} = 0.9$, and $k_{\text{rw},0} = 0.6$. Connate water and residual oil saturation are equal to 0.2. Capillary pressure is not included in the model. The initial pressure $p_0 = 100 \times 10^5$ Pa and the initial (connate) water saturation $S_0 = 0.2$, and both are uniform throughout the reservoir

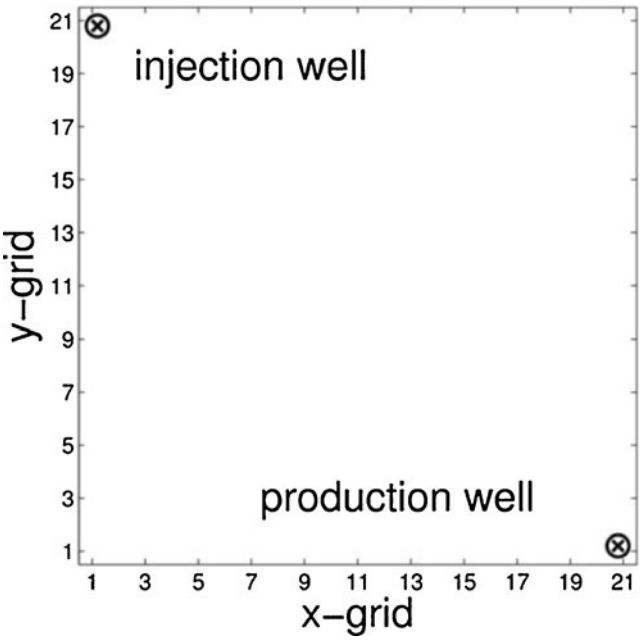

Fig. 1 Well locations for examples 1 and 2

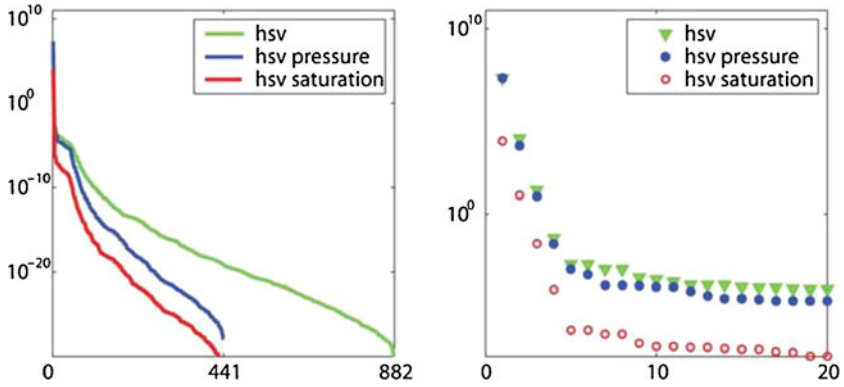

Fig. 2 Hankel singular values for example 1. *Left*: all singular values. *Right*: first 20 singular values

model. The reservoir model contains an injection well and a production well at opposite corners; see Fig. 1.

The inputs **u** represent the prescribed rate in the injection well (no pressure constraint) and the prescribed pressure in the production well (no rate constraint). The well indices are computed with a Peaceman model with well bore radius $r_w = 0.1$ m and no skin. Similarly as in reference [1], the nonzero entry in input matrix **B**, corresponding to the flow rate-controlled injection well, is scaled with $\mathbf{\Gamma}_u$ to the well index of the pressure-controlled production well. Both wells are assumed to be equipped with sensors to measure the bottom-hole pressure and the oil and water rates. The reservoir model is simulated for 10 years.

Since we consider the controllability and observability around a nominal input-state trajectory, we need to choose input signals c_j, as required in Eqs. 12 and 19, with magnitudes that can be considered as realistic during the operation of a petroleum reservoir. For this example, we have chosen pseudorandom binary signals (PRBS) with rate inputs between 0.4 and 0.5 m^3/s and pressure inputs between 90×10^5 and 99×10^5 Pa. The matrices $\mathbf{T}_l$ corresponding to a PRBS, as required in Eqs. 12, 18, and 19, are simply positive or negative unit matrices. The input signal is constant over intervals with a length of at least 25 time steps before it switches to another input level. Because we use a single signal, we have $r = s = 1$. Note that the use of

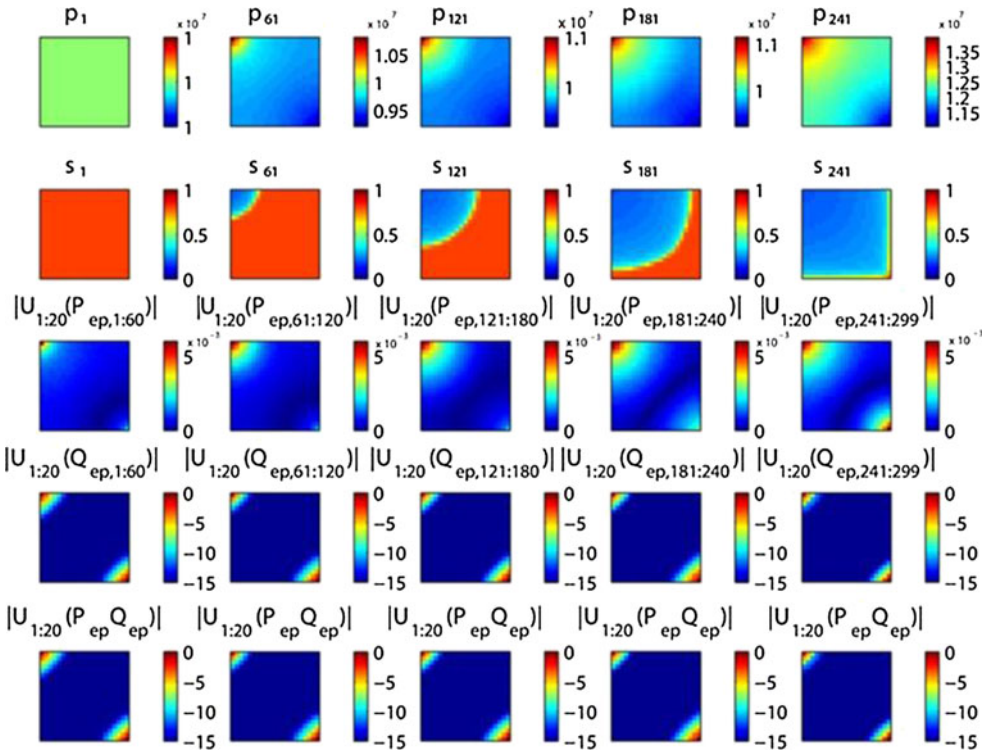

Fig. 3 Controllability and observability of the pressure states for example 1. *Columns* indicate five consecutive time intervals. The *top two rows* display the pressure and saturation fields, respectively. The *three bottom rows* display the (base 10) logarithm of the "weighted singular vectors" corresponding to the empirical controllability Gramian, the empirical observability Gramian, and the balanced Gramian, respectively

a PRBS implies that the inputs are piecewise constant, and that, strictly speaking, we do not compute empirical Gramians (for which we would need impulsive inputs for the controllability Gramian and no inputs for the observability Gramian) but "generalized empirical Gramians" or simply "empirical covariance matrices." This is tacitly assumed whenever we use the expression "empirical Gramian" in the discussion below.

Recall that the state vector $\mathbf{x}$ consists of stacked pressure and saturation vectors. The time scales of the dynamic behavior of the pressure and saturation states are very different from each other, as indicated by the clear separation in eigenvalues of the linearized system matrix $\bar{\mathbf{A}}_c$ (see Appendix and the discussion in Section 2.2). The pressure states of the linearized equations are associated with eigenvalues with high absolute values and exhibit a fast behavior, while the saturation states are associated with eigenvalues with very low values (in case of nonzero inputs) or even zero values (in the absence of inputs) and exhibit a very slow behavior. Therefore, only the results obtained with empirical Gramians will be presented.

For the first example, with a homogeneous permeability distribution, we computed the Hankel singular values of all states and of the pressure and saturation states separately using empirical Gramians; see Fig. 2. The values decrease rapidly, indicating that the reservoir model behaves as a model of much lower order than the order suggested by the number of states. Empirical controllability and observability Gramians were calculated for intervals around the nominal input-state trajectory, where $\check{\mathbf{x}}_0$ is chosen as the state vector in the middle of the interval. The interval length is chosen as 60 time steps. The results are shown in Fig. 3. The first two rows depict snapshots of pressures and saturations at the beginning of each of the five consecutive time intervals. The next three rows depict "weighted singular

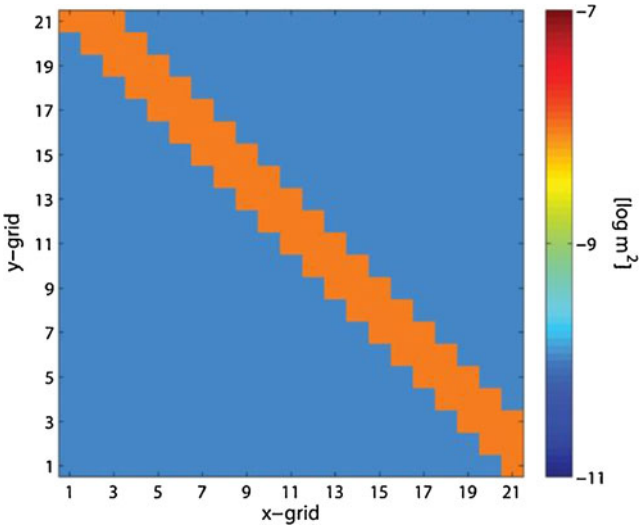

Fig. 5 Permeability field for example 2. Magnitude in ^{10}log, m^2

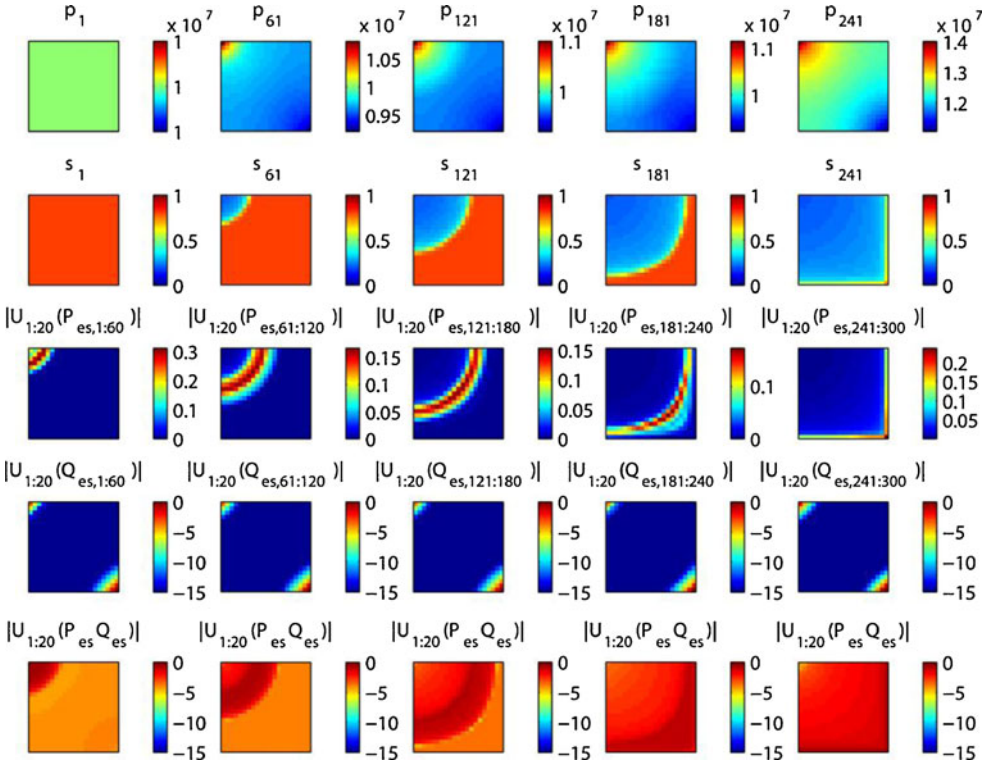

Fig. 4 Controllability and observability of the saturation states for example 1. Key as in Fig. 3

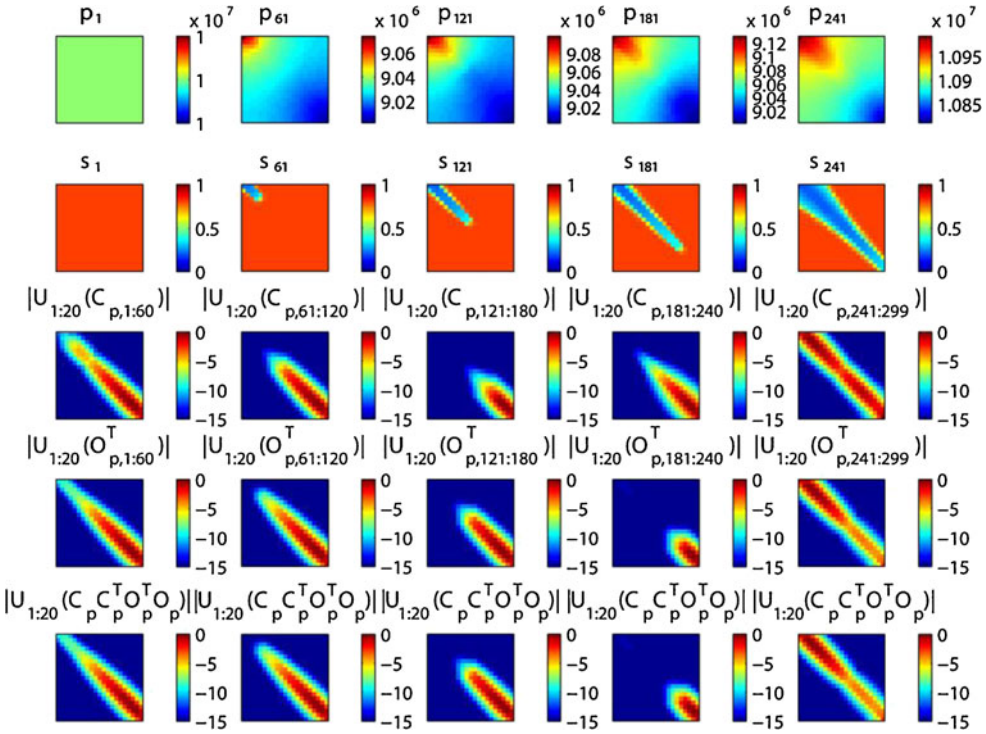

Fig. 6 Observability and controllability of pressure states for example 2. Key as in Fig. 3

vectors," as defined in Eq. 31, for the empirical controllability, observability, and balanced Gramians, respectively. The notation $|\mathbf{U}_{1:20}(\mathcal{P}_{e,1:60})|$ indicates the (base 10) logarithm of the weighted singular vector based on the first 20 columns of $\mathbf{U}$, obtained from the SVD of $\mathcal{P}_e$ computed over the time interval from 1 to 60 time steps. The key observation is that the pressures are most controllable around the wells. Also, after balancing, the pressures most relevant for

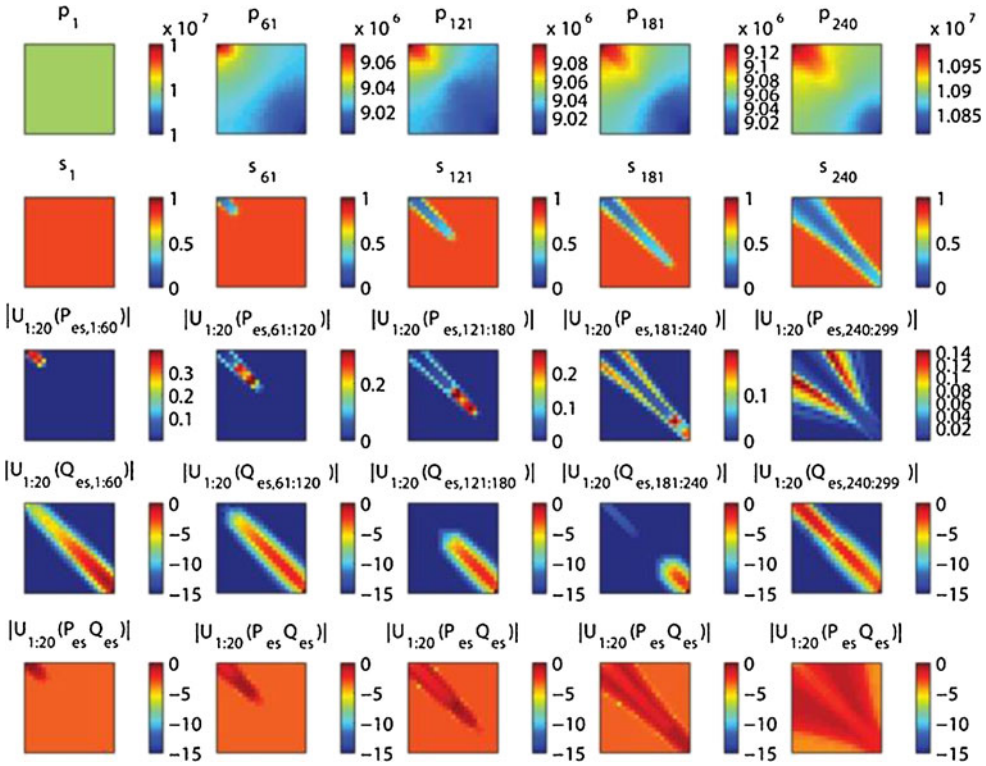

Fig. 7 Observability and controllability of saturation states for example 2. Key as in Fig. 3

the input–output behavior are located directly around the wells. This is completely in line with the observations for the single-phase reservoir models presented in reference [1].

Next, we analyze the controllability and observability of the saturation states with empirical controllability and observability Gramians. As before, these are calculated for consecutive "sliding" intervals with a length of 60 time steps. The first two rows in Fig. 4 show again the snapshots of pressure and saturation. The third row shows the weighted singular vector of the empirical controllability Gramian indicating that the saturation states are most controllable in the grid blocks where the fluid front is located. This is understandable since the saturation values around the front are the only values that change using the specific input signal. All other saturation values are either near their maximum value (upstream of the front) or at their minimum value (downstream of the front). The fourth row in Fig. 4 shows the weighted singular value of the empirical observability Gramian, indicating that the saturation in the grid blocks close to the wells are most observable. There seems to be no influence of the arrival of the saturation front on the observability. The fifth row shows the weighted value of the balanced states, indicating that the saturation states around the front are most relevant (i.e. least irrelevant) for the input–output behavior. Furthermore, upstream of the front, the states seem to be slightly more relevant than downstream of the front, since the values of the weighted singular vector are higher upstream of the front.

4.3 Example 2: heterogeneous permeability

As a next step, we analyzed the controllability and observability of a reservoir model with a heterogeneous permeability distribution in the form of a high-permeability streak or fracture from the injector to the producer with an absolute permeability of 10^{-8} m^2. The absolute permeability in the other grid blocks is 10^{-10} m^2; see Fig. 5. (We note that these values are unusually high; however, the results of our study are dependent on the permeability *contrast*, and the absolute values are therefore not relevant).

First, the controllability and observability of the pressure states are analyzed for this example. From Fig. 6, we can conclude that the pressure states are controllable around the wells and in the high-permeability streak downstream of the oil–water front. When the front has reached the producer, the most controllable states are again located around the wells and in the high-permeability streak. The most observable pressure states coincide with the most controllable pressure states. For this example, the pressure states that are most relevant for the input–output behavior are, according to the bottom row in Fig. 6, also located around the wells and in the high-permeability streak.

Next, the controllability and observability of the saturation states are analyzed. In Fig. 7, the results are shown. As in the previous case, the saturation states are most controllable around the oil–water front. The saturation states that are most observable are located close to the wells and furthermore in the high-permeability streak. The last row indicates that the saturation states around the front are most relevant (i.e. least irrelevant) for the input–output behavior.

5 Conclusions

In this work, the controllability and observability of the states (pressures and saturations) in two-phase (oil–water) reservoir models have been analyzed. For these nonlinear models, we analyzed the local controllability and observability around a nominal input-state trajectory with the aid of generalized empirical Gramians (covariance matrices).

Based on the analyzed examples, we conclude that the Hankel singular values of reservoir models decrease rapidly, indicating that these models are effectively of much lower order than the state-space models that results after spatial discretization. Furthermore, pressures are most controllable and observable around the wells that can control and observe the pressure states. The saturations are most controllable around the fluid front and most observable around the wells. After balancing the model, we can conclude that the most relevant (in terms of input–output behavior) pressure states are located around the wells and the most relevant saturation states are located around the fluid front.

From an example, with a heterogeneous permeability distribution, we can conclude that model parameters, such as permeability, that alter the shape and position of the fluid front, do influence the observability and controllability properties of the reservoir, and hence generalize the results. We conclude that the position of the wells and of the front between reservoir fluids, and to a lesser extent the position and shape of permeability heterogeneities, are the most important factors that determine the local controllability and observability properties of the reservoir. Therefore, research into effective reduced-order models for two-phase flow should focus on ways to capture, in some sense, the position of the fluid front(s).

Acknowledgments This research was carried out within the context of the Integrated Systems Approach to Petroleum Production (ISAPP) knowledge center. ISAPP is a joint project between Delft University of Technology (TU Delft), Shell International Exploration and Production, and the Netherlands Organization for Applied Scientific Research (TNO).

In Memoriam After preparation of this manuscript, the third author, Okko Bosgra, passed away too early on 21 February 2013. Prof. Okko Bosgra was one of the founders of our Dutch systems and control theory network. Through his role of bringing together mathematical systems theory and control engineering he has had a key role in establishing a strong national community with international recognition. The present paper is a clear example of his keen interest in combining system-theoretical aspects with industrial applications. We remember Okko as a passionate and sharp-minded scientist, an inspiring adviser, and an amicable colleague and friend.

Jorn Van Doren, Paul Van den Hof, Jan Dirk Jansen.

Appendix A: State-space formulation of two-phase porous media flow

This Appendix presents a derivation of the equations for flow through porous media in state-space form [34]. As an example, we consider two-phase (oil–water) isothermal, slightly compressible flow. Following the usual approach (see e.g., [35]), we can combine mass conservation equations and Darcy's law for each phase to obtain

$$-\nabla\cdot\left[\frac{\rho_i k_{ri}}{\mu_i}\mathbf{K}\left(\nabla p_i-\rho_i g\nabla d\right)\right]+\frac{\partial\left(\rho_i S_i\phi\right)}{\partial t}-\rho_i q_i'''=0, \tag{32}$$

where $\mathbf{K}$ is the permeability tensor, μ is fluid viscosity, k_r is relative permeability, p is pressure, g is acceleration of gravity, d is depth, ρ is fluid density, ϕ is porosity, S is fluid saturation, t is time, q''' is a source term expressed as flow rate per unit volume, and subscript $i\in\{o,w\}$ indicates the oil and water phases, respectively. Equations 32 (one for each phase) contain four unknowns, p_w, p_o, S_w, and S_o, two of which can be eliminated with aid of the relationships

$$S_w+S_o=1, \tag{33}$$

$$p_o-p_w=p_c(S_w), \tag{34}$$

where $p_c(S_w)$ is the oil–water capillary pressure. Substituting Eqs. 33 and 34 in Eq. 32, expanding the right-hand sides, applying chain-rule differentiation, and substituting isothermal oil, water, and rock compressibilities

$$c_o=\left.\frac{1}{\rho_o}\frac{\partial\rho_o}{\partial p_o}\right|_T, \tag{35}$$

$$c_w=\left.\frac{1}{\rho_w}\frac{\partial\rho_w}{\partial p_w}\right|_T\approx\left.\frac{1}{\rho_w}\frac{\partial\rho_w}{\partial p_o}\right|_T, \tag{36}$$

$$c_r=\frac{1}{\phi}\frac{\partial\phi}{\partial p_o}, \tag{37}$$

where T is temperature, allows us to express Eq. 32 in terms of p_o and S_w as follows:

$$-\nabla\cdot\left\{\frac{\rho_w k_{rw}}{\mu_w}\mathbf{K}\left[\left(\nabla p_o-\frac{\partial p_c}{\partial S_w}\nabla S_w\right)\right]\right\}+\rho_w\phi\left[S_w(c_w+c_r)\frac{\partial p_o}{\partial t}+\frac{\partial S_w}{\partial t}\right]-\rho_w q_w'''=0, \tag{38}$$

$$-\nabla\cdot\left[\frac{\rho_o k_{ro}}{\mu_o}\mathbf{K}\left(\nabla p_o-\rho_o g\nabla d\right)\right]+\rho_o\phi\left[\left(1-S_w\right)\left(c_o+c_r\right)\frac{\partial p_o}{\partial t}-\frac{\partial S_w}{\partial t}\right]-\rho_o q_o'''=0. \tag{39}$$

Equations 38 and 39 contain two state variables: the oil pressure p_o and the water saturation S_w. The equations are nonlinear because of the saturation dependency of the capillary pressure p_c and the relative permeabilities k_{ro} and k_{rw}. In the more general case, there may also be a pressure dependency of the densities ρ, the porosity ϕ, and the compressibilities c. In this paper, we considered, without loss of generality, a simplified case where gravity and capillary forces can be neglected. After semi-discretization of the equations in space, e.g., with a finite difference or finite element procedure, we obtain the following system of nonlinear first-order differential equations,

$$\underbrace{\begin{bmatrix}\mathbf{V}_{wp}(\mathbf{s}) & \mathbf{V}_{ws}\\ \mathbf{V}_{op}(\mathbf{s}) & \mathbf{V}_{os}\end{bmatrix}}_{\mathbf{V}}\begin{bmatrix}\dot{\mathbf{p}}\\ \dot{\mathbf{s}}\end{bmatrix}+\underbrace{\begin{bmatrix}\mathbf{T}_w(\mathbf{s}) & \mathbf{0}\\ \mathbf{T}_o(\mathbf{s}) & \mathbf{0}\end{bmatrix}}_{\mathbf{T}}\begin{bmatrix}\mathbf{p}\\ \mathbf{s}\end{bmatrix}=\underbrace{\begin{bmatrix}\mathbf{F}_w(\mathbf{s})\\ \mathbf{F}_o(\mathbf{s})\end{bmatrix}}_{\mathbf{F}}\mathbf{q}_{well,t}, \tag{40}$$

where $\mathbf{p}$ and $\mathbf{s}$ are vectors of pressures p_o and water saturations S_w in the grid block centers, $\mathbf{V}$ is an accumulation matrix (with entries that are functions of the porosity ϕ, and the oil, water, and rock compressibilities c_o, c_w, and c_r, respectively), $\mathbf{T}$ is a transmissibility matrix (with entries that are functions of the rock permeabilities k, the oil and water

relative permeabilities k_{ro} and k_{rw}, and the oil and water viscosities μ_o and μ_w), $\mathbf{F}$ is a fractional flow matrix (with entries that have functional dependencies similar to those of $\mathbf{T}$), and $\mathbf{q}_{well,t}$ is a vector of total well flow rates with nonzero values in those elements that correspond to grid blocks penetrated by a well. The matrices $\mathbf{V}$, $\mathbf{T}$, and $\mathbf{F}$ are all functions of $\mathbf{s}$, either directly or through the parameters. In the more general case of high compressibility, they are also a function of $\mathbf{p}$. The fractional flow matrices $\mathbf{F}_w$ and $\mathbf{F}_o$ are diagonal with fractional flows f_w and f_o as the elements that correspond to well grid blocks and zeros otherwise. In practice, the source terms are often not the flow rates in the wells but rather the pressures. This can be accounted for by rewriting Eq. 40 in partitioned form as [34]

$$\left[\begin{array}{ccc|ccc} \mathbf{V}_{wp,11} & 0 & 0 & \mathbf{V}_{ws,11} & 0 & 0 \\ 0 & \mathbf{V}_{wp,22} & 0 & 0 & \mathbf{V}_{ws,22} & 0 \\ 0 & 0 & \mathbf{V}_{wp,33} & 0 & 0 & \mathbf{V}_{ws,33} \\ \hline \mathbf{V}_{op,11} & 0 & 0 & \mathbf{V}_{os,11} & 0 & 0 \\ 0 & \mathbf{V}_{op,22} & 0 & 0 & \mathbf{V}_{os,22} & 0 \\ 0 & 0 & \mathbf{V}_{op,33} & 0 & 0 & \mathbf{V}_{os,33} \end{array}\right] \left[\begin{array}{c} \dot{\mathbf{p}}_1 \\ \dot{\mathbf{p}}_2 \\ \dot{\mathbf{p}}_3 \\ \hline \dot{\mathbf{s}}_1 \\ \dot{\mathbf{s}}_2 \\ \dot{\mathbf{s}}_3 \end{array}\right]$$

$$+ \left[\begin{array}{ccc|ccc} \mathbf{T}_{w,11} & \mathbf{T}_{w,12} & \mathbf{T}_{w,13} & 0 & 0 & 0 \\ \mathbf{T}_{w,21} & \mathbf{T}_{w,22} & \mathbf{T}_{w,23} & 0 & 0 & 0 \\ \mathbf{T}_{w,31} & \mathbf{T}_{w,32} & \mathbf{T}_{w,33} & 0 & 0 & 0 \\ \hline \mathbf{T}_{o,11} & \mathbf{T}_{o,12} & \mathbf{T}_{o,13} & 0 & 0 & 0 \\ \mathbf{T}_{o,21} & \mathbf{T}_{o,22} & \mathbf{T}_{o,23} & 0 & 0 & 0 \\ \mathbf{T}_{o,31} & \mathbf{T}_{o,32} & \mathbf{T}_{o,33} & 0 & 0 & 0 \end{array}\right] \left[\begin{array}{c} \mathbf{p}_1 \\ \mathbf{p}_2 \\ \mathbf{p}_3 \\ \hline \mathbf{s}_1 \\ \mathbf{s}_2 \\ \mathbf{s}_3 \end{array}\right]$$

$$= \left[\begin{array}{ccc|ccc} 0 & 0 & 0 & & & \\ 0 & \mathbf{F}_{w,22} & 0 & & & \\ 0 & 0 & \mathbf{F}_{w,33} & & & \\ \hline 0 & 0 & 0 & & & \\ 0 & \mathbf{F}_{o,22} & 0 & & & \\ 0 & 0 & \mathbf{F}_{o,33} & & & \end{array}\right] \left[\begin{array}{c} 0 \\ \breve{\mathbf{q}}_{well,t} \\ \mathbf{J}_3\left(\breve{\mathbf{p}} - \mathbf{p}_3\right) \end{array}\right]. \tag{41}$$

Here, the elements of vector $\mathbf{p}_1$ are the pressures in those grid blocks that are not penetrated by a well. The elements of $\mathbf{p}_2$ are the pressures in the blocks where the source terms are prescribed total well flow rates $\breve{\mathbf{q}}_{well,t}$, and those of $\mathbf{p}_3$ are the pressures in the blocks where the source terms are obtained through prescription of the bottom-hole pressures $\breve{\mathbf{p}}_{well}$ with the aid of a diagonal matrix of well indices $\mathbf{J}_3$. To compute the oil and water flow rates in the wells with prescribed pressures, we use the relationship

$$\left[\begin{array}{c} \overline{\mathbf{q}}_{well,w} \\ \overline{\mathbf{q}}_{well,o} \end{array}\right] = \left[\begin{array}{c} \mathbf{F}_{w,33} \\ \mathbf{F}_{o,33} \end{array}\right] \mathbf{J}_3\left(\breve{\mathbf{p}}_{well} - \mathbf{p}_3\right). \tag{42}$$

To compute the bottom-hole pressures $\overline{\mathbf{p}}_{well}$ in the wells with prescribed total flow rates, we need an additional diagonal matrix $\mathbf{J}_2$ of well indices such that

$$\breve{\mathbf{q}}_{well,t} = \mathbf{J}_2\left(\overline{\mathbf{p}}_{well} - \mathbf{p}_2\right), \tag{43}$$

from which we obtain

$$\overline{\mathbf{p}}_{well} = \mathbf{J}_2^{-1}\breve{\mathbf{q}}_{well,t} - \mathbf{p}_2. \tag{44}$$

To bring these equations in state-space form, we define the *state vector* $\mathbf{x}$, *input vector* $\mathbf{u}$, and *output vector* $\mathbf{y}$ as

$$\mathbf{u} \triangleq \left[\begin{array}{c} \breve{\mathbf{q}}_{well,t} \\ \breve{\mathbf{p}}_{well} \end{array}\right], \tag{45}$$

$$\mathbf{x} \triangleq \left[\begin{array}{c} \mathbf{p} \\ \mathbf{s} \end{array}\right] = \left[\begin{array}{c} \mathbf{p}_1 \\ \mathbf{p}_2 \\ \mathbf{p}_3 \\ \hline \mathbf{s}_1 \\ \mathbf{s}_2 \\ \mathbf{s}_3 \end{array}\right], \tag{46}$$

$$\mathbf{y} \triangleq \left[\begin{array}{c} \overline{\mathbf{p}}_{well} \\ \overline{\mathbf{q}}_{well,w} \\ \overline{\mathbf{q}}_{well,o} \end{array}\right]. \tag{47}$$

Equations 41, 42 and 44 can then be rewritten in nonlinear state-space form

$$\dot{\mathbf{x}} = \mathbf{f}(\mathbf{x}, \mathbf{u}) = \mathbf{A}_c(\mathbf{x})\,\mathbf{x} + \mathbf{B}_c(\mathbf{x})\,\mathbf{u}, \tag{48}$$

$$\mathbf{y} = \mathbf{h}(\mathbf{x}, \mathbf{u}) = \mathbf{C}(\mathbf{x})\,\mathbf{x} + \mathbf{D}(\mathbf{x})\,\mathbf{u}, \tag{49}$$

where the state-dependent matrices $\mathbf{A}_c(\mathbf{x})$, $\mathbf{B}_c(\mathbf{x})$, $\mathbf{C}(\mathbf{x})$ and $\mathbf{D}(\mathbf{x})$ are defined as

$$\mathbf{A}_c \triangleq -\mathbf{V}^{-1}\left[\begin{array}{ccc|ccc} \mathbf{T}_{w,11} & \mathbf{T}_{w,12} & \mathbf{T}_{w,13} & \mathbf{0} & \mathbf{0} & \mathbf{0} \\ \mathbf{T}_{w,21} & \mathbf{T}_{w,22} & \mathbf{T}_{w,23} & \mathbf{0} & \mathbf{0} & \mathbf{0} \\ \mathbf{T}_{w,31} & \mathbf{T}_{w,32} & \mathbf{T}_{w,33} + \mathbf{F}_{w,33}\mathbf{J}_3 & \mathbf{0} & \mathbf{0} & \mathbf{0} \\ \hline \mathbf{T}_{o,11} & \mathbf{T}_{o,12} & \mathbf{T}_{o,13} & \mathbf{0} & \mathbf{0} & \mathbf{0} \\ \mathbf{T}_{o,21} & \mathbf{T}_{o,22} & \mathbf{T}_{o,23} & \mathbf{0} & \mathbf{0} & \mathbf{0} \\ \mathbf{T}_{o,31} & \mathbf{T}_{o,32} & \mathbf{T}_{o,33} + \mathbf{F}_{o,33}\mathbf{J}_3 & \mathbf{0} & \mathbf{0} & \mathbf{0} \end{array}\right], \tag{50}$$

$$\mathbf{B}_c \triangleq \mathbf{V}^{-1}\left[\begin{array}{cc} \mathbf{0} & \mathbf{0} \\ \mathbf{F}_{w,22} & \mathbf{0} \\ \mathbf{0} & \mathbf{F}_{w,33}\mathbf{J}_3 \\ \hline \mathbf{0} & \mathbf{0} \\ \mathbf{F}_{o,22} & \mathbf{0} \\ \mathbf{0} & \mathbf{F}_{o,33}\mathbf{J}_3 \end{array}\right], \tag{51}$$

$$\mathbf{C} \triangleq \left[\begin{array}{ccc|ccc} \mathbf{0} & \mathbf{I} & \mathbf{0} & \mathbf{0} & \mathbf{0} & \mathbf{0} \\ \mathbf{0} & \mathbf{0} & -\mathbf{F}_{w,33}\mathbf{J}_3 & \mathbf{0} & \mathbf{0} & \mathbf{0} \\ \mathbf{0} & \mathbf{0} & -\mathbf{F}_{0,33}\mathbf{J}_3 & \mathbf{0} & \mathbf{0} & \mathbf{0} \end{array}\right], \tag{52}$$

$$\mathbf{D} \triangleq \left[\begin{array}{cc} \mathbf{J}_2^{-1} & \mathbf{0} \\ \mathbf{0} & \mathbf{F}_{w,33}\mathbf{J}_3 \\ \mathbf{0} & \mathbf{F}_{0,33}\mathbf{J}_3 \end{array}\right]. \tag{53}$$

The equations are nonlinear because almost all elements of the matrices $\mathbf{V}$, $\mathbf{T}$, $\mathbf{F}$, and $\mathbf{J}$ are functions of the states $\mathbf{x}$.

The equations are *control-affine* because they are linear in the controls $\mathbf{u}$. In the systems and control literature, $\mathbf{A}_c$ is usually called the *system matrix*, $\mathbf{B}_c$ the *input matrix*, $\mathbf{C}$ the *output matrix*, and $\mathbf{D}$ the *direct throughput matrix*. These matrices are normally applied in a linear setting, i.e., they are not supposed to be functions of $\mathbf{x}$. The inverse of the accumulation matrix $\mathbf{V}$ as required in Eqs. 50 and 51 can be computed at low computational costs because it consists of four diagonal sub-matrices. However, we emphasize that there is no need to perform the inverse operation if the equations serve as a basis for computation, and that the explicit state-space form (48) and its linearization (60) are only required for analysis of the system-theoretical properties of the equations.

We can linearize Eq. 48 in a point $\mathbf{x}^0$ or along an entire trajectory $\mathbf{x}^0(t)$ with the aid of the Taylor expansion

$$\dot{\mathbf{x}} = \mathbf{f}(\mathbf{u}, \mathbf{x}) \approx \mathbf{f}\left(\mathbf{u}^0, \mathbf{x}^0\right) + \frac{\partial \mathbf{f}\left(\mathbf{u}^0, \mathbf{x}^0\right)}{\partial \mathbf{u}}\left(\mathbf{u} - \mathbf{u}^0\right) + \frac{\partial \mathbf{f}\left(\mathbf{u}^0, \mathbf{x}^0\right)}{\partial \mathbf{x}}\left(\mathbf{x} - \mathbf{x}^0\right), \tag{54}$$

where we have neglected terms of second order and higher, and applied the usual short-cut notation

$$\frac{\partial \mathbf{f}\left(\mathbf{u}^0, \mathbf{x}^0\right)}{\partial \mathbf{x}} \triangleq \left.\frac{\partial \mathbf{f}(\mathbf{u}, \mathbf{x})}{\partial \mathbf{x}}\right|_{\mathbf{u}=\mathbf{u}^0,\, \mathbf{x}=\mathbf{x}^0}. \tag{55}$$

Defining

$$\overline{\mathbf{u}} \triangleq \mathbf{u} - \mathbf{u}^0, \tag{56}$$

$$\overline{\mathbf{x}} \triangleq \mathbf{x} - \mathbf{x}^0, \tag{57}$$

Eq. 54 can be rewritten as

$$\dot{\overline{\mathbf{x}}} + \dot{\mathbf{x}}^0 \approx \mathbf{f}\left(\mathbf{u}^0, \mathbf{x}^0\right) + \frac{\partial \mathbf{f}\left(\mathbf{u}^0, \mathbf{x}^0\right)}{\partial \mathbf{u}}\overline{\mathbf{u}} + \frac{\partial \mathbf{f}\left(\mathbf{u}^0, \mathbf{x}^0\right)}{\partial \mathbf{x}}\overline{\mathbf{x}}, \tag{58}$$

which, because

$$\dot{\mathbf{x}}^0 = \mathbf{f}\left(\mathbf{u}^0, \mathbf{x}^0\right), \tag{59}$$

can be reduced to the linearized system equations

$$\dot{\overline{\mathbf{x}}} = \overline{\mathbf{A}}_c\left(\mathbf{u}^0, \mathbf{x}^0\right)\overline{\mathbf{x}} + \overline{\mathbf{B}}_c\left(\mathbf{x}^0\right)\overline{\mathbf{u}}, \tag{60}$$

where the Jacobian matrices $\overline{\mathbf{A}}_c$ and $\overline{\mathbf{B}}_c$ are defined as

$$\overline{\mathbf{A}}_c\left(\mathbf{u}^0, \mathbf{x}^0\right) \triangleq \frac{\partial \mathbf{f}\left(\mathbf{u}^0, \mathbf{x}^0\right)}{\partial \mathbf{x}} = \mathbf{A}_c\left(\mathbf{x}^0\right) + \frac{\partial \mathbf{A}_c(\mathbf{x}0)}{\partial \mathbf{x}}\mathbf{x}^0 + \frac{\partial \mathbf{B}_c\left(\mathbf{x}^0\right)}{\partial \mathbf{x}}\mathbf{u}^0, \tag{61}$$

$$\overline{\mathbf{B}}_c\left(\mathbf{x}^0\right) \triangleq \frac{\partial \mathbf{f}\left(\mathbf{u}^0, \mathbf{x}^0\right)}{\partial \mathbf{u}} = \mathbf{B}_c\left(\mathbf{x}^0\right). \tag{62}$$

In a similar fashion, we can linearize the nonlinear output Eq. 49 to obtain

$$\overline{\mathbf{y}} = \overline{\mathbf{C}}\left(\mathbf{u}^0, \mathbf{x}^0\right)\overline{\mathbf{x}} + \overline{\mathbf{D}}\left(\mathbf{x}^0\right)\overline{\mathbf{u}}, \tag{63}$$

where the Jacobian matrices $\overline{\mathbf{C}}$ and $\overline{\mathbf{D}}$ are defined as

$$\overline{\mathbf{C}}\left(\mathbf{u}^0, \mathbf{x}^0\right) \triangleq \frac{\partial \mathbf{h}\left(\mathbf{u}^0, \mathbf{x}^0\right)}{\partial \mathbf{x}} = \mathbf{C}\left(\mathbf{x}^0\right) + \frac{\partial \mathbf{C}\left(\mathbf{x}^0\right)}{\partial \mathbf{x}}\mathbf{x}^0 + \frac{\partial \mathbf{D}\left(\mathbf{x}^0\right)}{\partial \mathbf{x}}\mathbf{u}^0, \tag{64}$$

$$\overline{\mathbf{D}}\left(\mathbf{x}^0\right) \triangleq \frac{\partial \mathbf{h}\left(\mathbf{u}^0, \mathbf{x}^0\right)}{\partial \mathbf{u}} = \mathbf{D}\left(\mathbf{x}^0\right). \tag{65}$$

Using an explicit time discretization, Eqs. 48 and 49 can be rewritten in discrete-time form as

$$\mathbf{x}_{k+1} = \mathbf{A}(\mathbf{x}_k)\,\mathbf{x}_k + \mathbf{B}(\mathbf{x}_k)\,\mathbf{u}_k, \tag{66}$$

$$\mathbf{y}_k = \mathbf{C}(\mathbf{x}_k)\,\mathbf{x}_k + \mathbf{D}(\mathbf{x}_k)\,\mathbf{u}_k, \tag{67}$$

where

$$\mathbf{A}(\mathbf{x}_k) = (\mathbf{I} + \Delta t \mathbf{A}_c(\mathbf{x}_k)), \tag{68}$$

$$\mathbf{B}(\mathbf{x}_k) = \Delta t \mathbf{B}_c(\mathbf{x}_k). \tag{69}$$

Here, we apply the usual notation $\mathbf{x}_k$ to indicate $\mathbf{x}(k\Delta t)$, where the subscript k is the time step counter or discrete time. In a similar fashion, Eqs. 60 and 63 can be written in discrete-time form as

$$\overline{\mathbf{x}}_{k+1} = \overline{\mathbf{A}}\left(\mathbf{u}^0, \mathbf{x}^0\right)\overline{\mathbf{x}}_k + \overline{\mathbf{B}}\left(\mathbf{x}^0\right)\overline{\mathbf{u}}_k, \tag{70}$$

and

$$\overline{\mathbf{y}}_k = \overline{\mathbf{C}}\left(\mathbf{u}^0, \mathbf{x}^0\right)\overline{\mathbf{x}}_k + \overline{\mathbf{D}}\left(\mathbf{x}^0\right)\overline{\mathbf{u}}_k. \tag{71}$$

The discretization time step is chosen as

$$\Delta t = \frac{0.5}{|\lambda_{\min}(\mathbf{A}_c)|}, \tag{72}$$

where $\lambda_{\min}$ represents the most negative eigenvalue. This theoretical results leads to quite small time steps and is referred to as the so-called Nyquist–Shannon sampling time needed to accurately capture all of the dynamics in Eq. 48; see e.g., [36]. We note that both the theory and results in the paper do not depend on implicit or explicit time discretization or on the particular value of the discretization time step Δt, and also apply to the continuous-time case. In the numerical examples, we therefore used an implicit

scheme with time steps considerably larger than the theoretical minimum given by Eq. 72. We verified that reduction of the time step size did not lead to a change in the results.

References

1. Zandvliet, M.J., Van Doren, J.F.M., Bosgra, O.H., Jansen, J.D., Van den Hof, P.M.J.: Controllability, observability and identifiability in single-phase porous media flow. Comput. Geosci. **12**(4), 605–622 (2008)
2. Sudaryanto, B., Yortsos, Y.C.: Optimization of fluid front dynamics in porous media using rate control. Phys. Fluids **12**(7), 1656–70 (2000)
3. Fyrozjaee, M.H., Yortsos, Y.C.: Control of a displacement front in potential flow using flow-rate partition. Paper SPE 99524, presented at the SPE intelligent energy conference, Amsterdam, The Netherlands
4. Ramakrishnan, T.S.: On reservoir fluid-flow control with smart completions. SPE Prod. Oper. **22**(1), 4–12 (2007)
5. Jansen, J.D., Bosgra, O.H., van den Hof, P.M.J.: Model-based control of multiphase flow in subsurface oil reservoirs. J. Process Control **18**, 846–855 (2008)
6. Jansen, J.D., Van Doren, J.F.M., Heidary-Fyrozjaee, M., Yortsos, Y.C.: Front controllability in two-phase porous media flow. In: Van den Hof, P.M.J., Scherer, C., Heuberger, P.S.C. (eds.) Model-based Control—Bridging Rigorous Theory and Advanced Control, pp. 203–219. Springer, New York (2009)
7. Jansen, J.D.: Adjoint-based optimization of multiphase flow through porous media—a review. Comput. Fluids **46**(1), 40–51 (2011)
8. Watson, A.T., Gavalas, G.R., Seinfeld, J.H.: Identifiability of estimates of two-phase reservoir properties in history matching. SPE J. **24**(6), 697–706 (1984)
9. Datta-Gupta, A., Vasco, D.W., Long, J.C.S.: On the sensitivity and spatial resolution of transient pressure and tracer data for heterogeneity characterization. SPE Form. Eval. **12**(2), 137–144 (1997)
10. Oliver, D.S., Reynolds, A.C., Liu, N.: Inverse theory for petroleum reservoir characterization and history matching. Cambridge University Press, Cambridge (2008)
11. Van Doren, J.F.M., Van den Hof, P.M.J., Jansen, J.D., Bosgra, O.H.: Determining identifiable parameterizations for large-scale physical models in reservoir engineering. In: Chung, M., Misra, P., Shim, H. (eds.) Proceedings 17th International Federation for Automatic Control (IFAC) World Congress, pp. 11421–11426. Seoul, 6–11 July 2008
12. Van Doren, J.F.M., Douma, S.G., Van den Hof, P.M.J., Jansen, J.D., Bosgra, O.H.: Identifiability: from qualitative analysis to model structure approximation. In: Proceedings 15th IFAC Symposium on System Identification (SYSID), St. Malo, 6–8 July 2009
13. Oliver, D.S., Chen, Y.: Recent progress on reservoir history matching: a review. Comput. Geosci. **15**(1), 185–221 (2011)
14. Vakili-Ghahani, S.A., Jansen, J.D.: Control-relevant upscaling. SPE J. **15**(2), 471–479 (2010)
15. Vakili-Ghahani, S.A., Jansen, J.D.: A system-theoretical approach to selective grid coarsening of reservoir models. Comput. Geosci. **16**(1), 159–176 (2012)
16. Heijn, T., Markovinovi, R., Jansen, J.D.: Generation of low-order reservoir models using system-theoretical concepts. SPE J. **9**(2), 202–218 (2004)
17. Van Doren, J.F.M., Markovinović, R., Jansen, J.D.: Reduced-order optimal control of waterflooding using POD. Comput. Geosci. **10**(1), 137–158 (2006)
18. Cardoso, M.A., Durlofsky, L.J., Sarma, P.: Development and application of reduced-order modeling procedures for subsurface flow simulation. Int. J. Numer. Methods Eng. **77**(9), 1322–1350 (2009)
19. Wu, Z., Reynolds, A.C., Oliver, D.S.: Conditioning geostatistical models to two-phase production data. SPE J. **4**(2), 144–152 (1999)
20. Rodrigues, J.R.P.: Calculating derivatives for automatic history matching. Comput. Geosci. **10**(1), 119–136 (2006)
21. Tavakoli, R., Reynolds, A.C.: History matching with parameterization based on the SVD of a dimensionless sensitivity matrix. SPE J. **15**(2), 495–508 (2010)
22. Nijmeijer, H., Van der Schaft, A.: Nonlinear Dynamical Control Systems. Springer, New York (1996)
23. Hermann, R., Krener, A.J.: Nonlinear controllability and observability. IEEE Trans. Autom. Control **22**(5), 728 (1997)
24. Isidori, A.: Nonlinear Control Systems. Springer, New York (1995)
25. Lall, S., Marsden, J.E., Glavaski, S.A.: A subspace approach to balanced truncation for model reduction of nonlinear control systems. Int. J. Robust Nonlinear Control **12**(5), 519–535 (2002)
26. Hahn, J., Edgar, T.F., Marquardt, W.: Controllability and observability covariance matrices for the analysis and order reduction of stable nonlinear systems. J. Process Control **13**(2), 115–127 (2003)
27. Kailath, T.: Linear Systems. Prentice-Hall, Englewood Cliffs (1980)
28. Willcox, K., Peraire, J.: Balanced model reduction via the proper orthogonal decomposition. J. Am. Inst. Aeronaut. Astronaut. **40**(11), 2323–2330 (2002)
29. Rowley, C.W.: Model reduction for fluids, using balanced proper orthogonal decomposition. Int. J. Bifurcation Chaos **15**(3), 997–1013 (2005)
30. Moore, B.C.: Principal component analysis in linear systems: controllability, observability, and model reduction. IEEE Trans. Automat. Control **26**(1), 17–32 (1981)
31. Antoulas, A.C.: Approximation of Large-scale Dynamical Systems. SIAM, Philadelphia (2005)
32. Verriest, E.I., Kailath, T.: On generalized balanced realizations. IEEE Trans. Automat. Control **28**(8), 833–844 (1983)
33. Van Doren, J.F.M.: Model structure analysis for model-based operation of petroleum reservoirs. PhD thesis, Delft University of Technology (2010)
34. Jansen, J.D.: A systems description of flow through porous media. Springer Briefs in Earth Sciences (2013)
35. Aziz, K., Settari, A.: Petroleum Reservoir Simulation. Applied Science Publishers, London (1979)
36. Astrom, K.J., Wittenmark, B., 2nd ed.: Computer Controlled Systems. Prentice Hall, Englewood Cliffs (1990)